

Local curvature and stability of two-dimensional systems

Jie Guan,¹ Zhongqi Jin,² Zhen Zhu,¹ Chern Chuang,³ Bih-Yaw Jin,⁴ and David Tománek^{1,*}¹*Physics and Astronomy Department, Michigan State University, East Lansing, Michigan 48824, USA*²*Chemistry Department, Michigan State University, East Lansing, Michigan 48824, USA*³*Department of Chemistry, Massachusetts Institute of Technology, Cambridge, MA 02139, USA*⁴*Department of Chemistry and Center for Emerging Material and Advanced Devices, National Taiwan University, Taipei 10617, Taiwan*

(Dated: March 6, 2022)

We propose a fast method to determine the local curvature in two-dimensional (2D) systems with arbitrary shape. The curvature information, combined with elastic constants obtained for a planar system, provides an accurate estimate of the local stability in the framework of continuum elasticity theory. Relative stabilities of graphitic structures including fullerenes, nanotubes and schwarzites, as well as phosphorene nanotubes, calculated using this approach, agree closely with *ab initio* density functional calculations. The continuum elasticity approach can be applied to all 2D structures and is particularly attractive in complex systems with known structure, where the quality of parameterized force fields has not been established.

PACS numbers: 61.48.De, 68.55.ap, 61.46.-w, 81.05.ub

I. INTRODUCTION

Layered structures including graphite, hexagonal boron nitride, black phosphorus, transition metal dichalcogenides such as MoS₂, and oxides including V₂O₅ are very common in Nature. The possibility to form stable two-dimensional (2D) structures by mechanical exfoliation of these structures appears very attractive for a variety of applications.^{1,2} The most prominent example of such 2D systems, graphitic carbon, is the structural basis not only of graphene,¹ but also fullerenes, nanotubes, tori and schwarzites.³⁻⁷ Even though the structural motif in all of these systems may be the same, their mechanical and electronic properties depend sensitively on the local morphology.⁸⁻¹⁰ Not only does the natural abundance of structural allotropes and isomers reflect their net energetic stability, but also the relative chemical reactivity of specific sites in a given structure correlates well with the local curvature and local stability.⁸⁻¹⁰ This relationship has been well established for the reactive sites in the C₅₀ fullerene,⁸ used to induce structural collapse leading to chemical unzipping of carbon nanotubes,¹¹⁻¹³ and to destroy collapsed carbon nanotubes.¹⁰

For very large structures, estimating the global or local stability using *ab initio* calculations has proven impracticable. There, the stability has often been estimated using empirical rules or parameterized force fields including the Tersoff potential and molecular mechanics,¹⁴⁻¹⁷ with sometimes unsatisfactory results. Application of continuum elasticity theory, which can describe stability changes due to deviation from planarity, has been successful, but limited to systems with a well-defined, constant curvature.^{18,19} Since strain energy is local and independent of the global morphology, it is intriguing to explore, whether the local deformation energy may be accurately determined from local morphology estimates using the atomic geometry. If so, then the local stability

in even arbitrarily shaped structures could be estimated accurately.

Here we propose a fast method to determine the local curvature in 2D systems with a complex morphology using the local atomic geometry. Curvature information alone, combined with elastic constants obtained for a planar system, provides accurate stability estimates in the framework of continuum elasticity theory. We find that relative stabilities of graphitic structures including fullerenes, nanotubes and schwarzites, as well as phosphorene nanotubes, calculated using this approach, agree closely with *ab initio* density functional calculations. The

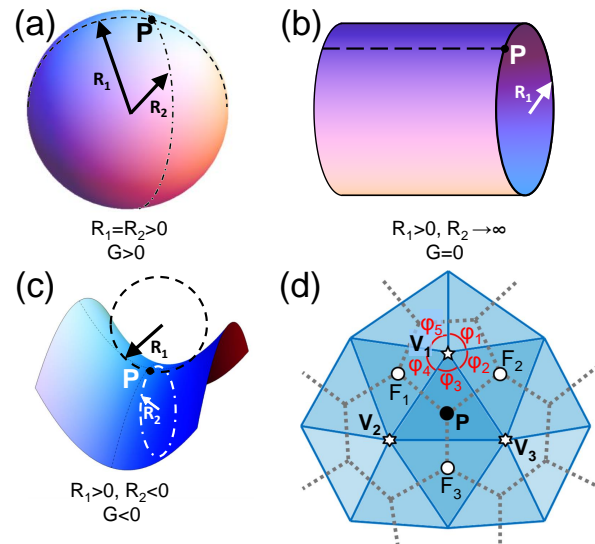


FIG. 1. (Color online) Principal radii of curvature R_1, R_2 and the Gaussian curvature G on the surface of (a) a sphere, (b) a cylinder and (c) in a saddle point. (d) Determination of the local curvature at point P using the atomic lattice and the dual lattice.

continuum elasticity approach can be applied to all 2D structures and is particularly attractive in complex systems with known structure, where the quality of parameterized force fields has not been established.

II. LOCAL CURVATURE AND CURVATURE ENERGY

The local curvature at a particular location on a surface is given by the two principal radii of curvature R_1 and R_2 , as shown in Fig. 1. On a spherical surface, $R_1 = R_2$. On a cylindrical surface, R_1 is the cylinder radius and $R_2 \rightarrow \infty$. Finally, a saddle point on a surface is characterized by opposite signs of R_1 and R_2 . Knowing the principal radii of curvature everywhere, we may use continuum elasticity theory to determine the curvature energy ΔE_C with respect to a planar layer using²⁰

$$\Delta E_C = \frac{1}{2}D \int_{surface} dA \left(\frac{1}{R_1^2} + \frac{1}{R_2^2} + \frac{2\alpha}{R_1 R_2} \right). \quad (1)$$

Here, the integral extends across the entire closed surface, D is the flexural rigidity and α is the Poisson ratio. Simple expressions for ΔE_C can be obtained for simple morphologies such as a sphere or a cylinder, where R_1 and R_2 are constant everywhere.¹⁸ This is, however, not the case in general.

We find it convenient to introduce the local mean curvature

$$k = \frac{1}{2} \left(\frac{1}{R_1} + \frac{1}{R_2} \right) \quad (2)$$

and the local Gaussian curvature

$$G = \frac{1}{R_1 R_2}. \quad (3)$$

Using these quantities, we can rewrite Eq. (1) as

$$\Delta E_C = D \int_{surface} dA [2k^2 - (1 - \alpha)G]. \quad (4)$$

In the following, we will consider the equilibrium arrangement of atoms in a planar 2D structure as the reference structure and will determine the local curvature from changes in the local morphology. The discrete counterpart of Eq. (4) for the curvature energy ΔE_C is a sum over atomic sites i ,

$$\Delta E_C \approx DA \sum_i [2k_i^2 - (1 - \alpha)G_i], \quad (5)$$

where A is the area per atom.

To use Eq. (5) for curvature energy estimates, we need to know the local curvatures k and G at all atomic sites. Our approach to estimate these values at a given site P is illustrated in Fig. 1(d). According to Eq. (2), the local

mean curvature k should be close to the average inverse radius of curvature at that point,

$$k \approx \left\langle \frac{1}{R} \right\rangle. \quad (6)$$

Since the atomic site P and its nearest three neighbors F_1 , F_2 and F_3 define the surface of a sphere of radius R , we take $k = 1/R$.

The positions of four atoms do not allow to distinguish, whether P is on a plane, a sphere, a cylinder, or in a saddle point. We may obtain this additional information using the concept of angular defect. On any surface, which can be triangulated as shown in Fig. 1(d), the angular defect at a representative vertex V_1 is defined by $\Delta(V_1) = 2\pi - \sum_i \varphi_i$ in radian units. The local Gaussian curvature at V_1 is then given by²¹

$$G(V_1) = \Delta(V_1)/A_t = \left(2\pi - \sum_i \varphi_i \right) / A_t, \quad (7)$$

where A_t is the total area of the triangulated surface divided by the number of vertices.

For trivalent molecular graphs containing 5-, 6- and 7-membered rings found in fullerenes, carbon nanotubes and schwarzites, a unique triangulation may be obtained by connecting the centers of adjacent polygons. This method is referred to as the dual graph in graph theory²² and its use is illustrated in Fig. 1(d). Since P is not a vertex in the dual graph, but rather the center of the triangle $\Delta V_1 V_2 V_3$, we must infer the local Gaussian curvature at P from the angular defects at V_1 , V_2 and V_3 . If vertex V_j is surrounded by n_j triangles, we may assign to point P the angular defect $\Delta(P) = \Delta(V_1)/n_1 + \Delta(V_2)/n_2 + \Delta(V_3)/n_3$. Then, we can estimate the local Gaussian curvature at P as

$$G(P) = \Delta(P)/A, \quad (8)$$

where A is the average area per atom. We use $A = 2.62 \text{ \AA}^2$, the value found in the honeycomb lattice of graphene, for all graphitic structures.

The above definition of the local Gaussian curvature satisfies exactly the equality

$$A \sum_{atoms} G(P_j) = A_t \sum_{vertices} G(V_j) = 2\pi\chi. \quad (9)$$

Here, χ is the Euler characteristic of the surface, given by $\chi = 2 - 2g$, where g is the genus, meaning ‘number of holes’. Of interest here is the fact that $\chi = 2$ for spherical objects like fullerenes and $\chi = 0$ for cylindrical objects such as nanotubes. Equation (9) is the discretized version of the Gauss-Bonnet theorem²³ regarding the integral of the Gaussian curvature over an entire closed surface, called the sum of the defect, which is usually formulated as $\int_{surface} G dA = 2\pi\chi$.

The variation of the local Gaussian curvature G and the local curvature energy $\Delta E_C/A$ across the surface

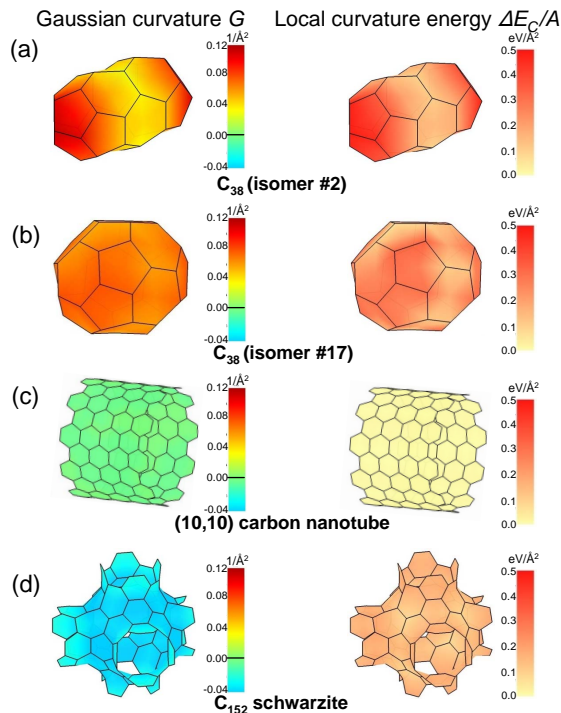


FIG. 2. (Color online) Local Gaussian curvature G (left panels) and local curvature energy $\Delta E_C/A$ across the surface of (a) the least stable C_{38} isomer, (b) the most stable C_{38} isomer, (c) a (10,10) carbon nanotube, and (d) a schwarzite structure with 152 atoms per unit cell. The values of G and $\Delta E_C/A$ have been interpolated across the surface.

of carbon polymorphs, including two fullerene isomers discussed in Section III.B, a nanotube and a schwarzite structure, is displayed in Fig. 2. The local curvature energy in these sp^2 -bonded structures has been evaluated using the elastic constants of graphene¹⁸ $D = 1.41$ eV and $\alpha = 0.165$. The higher stability of the $C_{38}(17)$ isomer in Fig. 2(b) is reflected in a rather uniform curvature energy and Gaussian curvature distribution. The low stability of the $C_{38}(2)$ isomer in Fig. 2(a) is reflected in a large variation of curvature energy and Gaussian curvature, clearly indicating the most reactive sites. Cylindrical carbon nanotubes, such as the (10,10) nanotube displayed in Fig. 2(c), have zero Gaussian curvature and a constant curvature energy caused by the mean curvature. Schwarzites such as the C_{152} structure, displayed in Fig. 2(d), have only negative Gaussian curvature that may vary across the surface, causing variations in the local curvature energy.

III. VALIDATION OF THE CONTINUUM ELASTICITY APPROACH

We will next test the accuracy of the continuum elasticity approach by calculating the relative stability of non-planar structures based on graphitic carbon. An infinite

number of morphologies including nanotubes, fullerenes and schwarzites may be produced by deforming a segment of a graphene layer and reconnecting its edges so that all carbon atoms are threefold coordinated. In many cases, the non-planar structures contain carbon pentagons and heptagons in the graphitic honeycomb arrangement of atoms as required by Euler's theorem.²³

To validate the continuum elasticity theory results, we calculated the total energy of a graphene monolayer and selected graphitic structures using *ab initio* density functional theory (DFT) as implemented in the SIESTA code.²⁴ We used the Local Density Approximation (LDA)^{25,26} and Perdew-Burke-Ernzerhof (PBE)²⁷ exchange-correlation functionals, norm-conserving Troullier-Martins pseudopotentials²⁸, and a double- ζ basis including polarization orbitals. The 1D Brillouin zone of nanotubes was sampled by 16 k -points and the 2D Brillouin zone of graphene by 16×16 k -points.²⁹ The small Brillouin zones of schwarzites with several hundred C atoms per unit cell were sampled by only 1 k -point. We used a mesh cutoff energy of 180 Ry to determine the self-consistent charge density, which provided us with a precision in total energy of $\lesssim 2$ meV/atom. All geometries have been optimized using the conjugate gradient method,³⁰ until none of the residual Hellmann-Feynman forces exceeded 10^{-2} eV/Å.

A. DFT results for fullerenes

Our DFT-LDA results for the relative energy ΔE_{tot}^{DFT} of optimized C_n fullerenes^{31,32} with respect to graphene are shown in Fig. 3(a). The various data points for one size correspond to different structural isomers, which are increasing fast in number with increasing n . If all fullerenes were perfect spheres, Eq. (4) would simplify to¹⁸ $\Delta E_C = 4\pi D(1 + \alpha)$. Using the proper elastic constants for graphene¹⁸ $D = 1.41$ eV and $\alpha = 0.165$, we would estimate $\Delta E_C = 20.6$ eV for all fullerenes independent of size. The numerical values for the different optimized fullerene isomers in Fig. 3(a) are all larger, indicating that variations in the local curvature and bond lengths cause a significant energy penalty.

B. Comparison between computational approaches for C_{38} fullerene isomers

As we show in the following, considering only local curvature variations across the surface (and ignoring precise atomic positions) allows continuum elasticity theory to quantitatively predict the strain energy with a precision competing with *ab initio* calculations. To illustrate this point, we present in Fig. 3(b) the total strain energy ΔE in seventeen isomers of C_{38} obtained using various approaches. The strain energy ΔE_{tot}^{DFT} based on DFT, which is expected to represent closely the experimental results, is not only significantly lower than the predicted

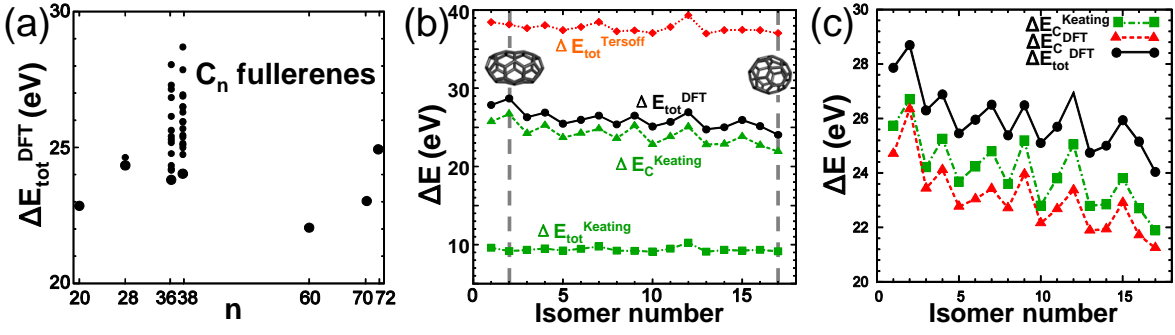


FIG. 3. (Color online) Strain energy ΔE in carbon nanostructures with respect to the graphene reference system. (a) DFT-based total strain energy ΔE_{tot}^{DFT} for selected fullerenes, with the most stable isomers indicated by the larger symbols. (b) Strain energy ΔE in different C_{38} isomers. Total energy differences ΔE_{tot}^{DFT} based on DFT, $\Delta E_{tot}^{Tersoff}$ based on the Tersoff potential and $\Delta E_{tot}^{Keating}$ based on the Keating potential are compared to curvature energies $\Delta E_C^{Keating}$ based on Keating-optimized geometries. (c) Strain energy ΔE in different C_{38} isomers. DFT total energies ΔE_{tot}^{DFT} are compared to curvature energies ΔE_C^{DFT} based on continuum elasticity theory for structures optimized by DFT, and $\Delta E_C^{Keating}$ values based on continuum elasticity theory for structures optimized using the Keating potential.

values $\Delta E_{tot}^{Tersoff}$ based on the Tersoff potential,¹⁴ but also differs from this popular bond-order potential in the prediction of relative stabilities.

Next we demonstrate that accurate energy estimates may be obtained even for geometries optimized using simple potentials with only bond stretching and bond bending terms such as the Keating potential^{33,34}

$$\Delta E_K = \frac{1}{2}\alpha_K \sum_{\substack{\langle i,j \rangle \\ i < j}} \frac{(r_{ij}^2 - R^2)^2}{R^2} + \frac{1}{2}\beta_K \sum_{\substack{\langle i,j,k \rangle \\ j < k}} \frac{(\mathbf{r}_{ij} \cdot \mathbf{r}_{ik} + \frac{1}{2}R^2)^2}{R^2}. \quad (10)$$

The first term sums over nearest neighbor pairs and the second term over nearest neighbor triplets, where j and k share the same neighbor i . DFT calculations for graphene yield $R = 1.42 \text{ \AA}$ as bond length, 120° as bond angle, $\alpha_K = 11.28 \text{ eV/\AA}^2$ and $\beta_K = 4.14 \text{ eV/\AA}^2$.

Geometries of C_{38} fullerene isomers optimized by DFT and the Keating potential are presented in the Supplemental Material.³² Strain energies for Keating optimized fullerenes are shown in Fig. 3(b). Whereas the Keating optimized geometry is close to the DFT optimized geometry, the Keating strain energy $\Delta E_{tot}^{Keating}$ clearly underestimates the DFT values and does not correctly represent the relative stabilities of the different isomers. As an alternative, we used the Keating optimized geometry to obtain the curvature strain energy $\Delta E_C^{Keating}$ using the continuum approach. We found that this approach represents the relative stabilities of isomers adequately and compares well to ΔE_{tot}^{DFT} . The curvature strain energy values are somewhat lower than the DFT values, since energy penalties associated with bond stretching and bending do not appear in the continuum approach. The small value of such corrections reflects the fact that in equilibrated structures, bond lengths and angles are near their optimum. The largest errors are expected in frustrated structures, where not all bond lengths and angles can be optimized simultaneously.

One of the key findings of this study is that continuum elasticity theory provides not only a fast, but also a relatively robust way to determine relative stabilities that are, to some degree, insensitive to the precise geometry. We illustrate this point in Fig. 3(c), where we compare different ways to determine the total strain energy ΔE in all C_{38} isomers discussed in Fig. 3(b). ΔE_{tot}^{DFT} , shown by the solid line, is the difference between the total energy in DFT of DFT-optimized C_{38} isomers and 38 carbon atoms in the graphene structure. ΔE_C^{DFT} , given by the dashed line, is the curvature energy based on the DFT-optimized geometry. $\Delta E_C^{Keating}$, given by the dash-dotted line, is the curvature energy based on the Keating-optimized geometry. We note that all expressions provide an accurate representation of relative stabilities. As mentioned above, the fact that ΔE_C is about 10% lower than ΔE_{tot} is caused by our neglecting the stretching and bending of discrete atomic bonds in the continuum approach.

C. Comparison of computational approaches for sp^2 bonded carbon nanostructures

Encouraged by the level of agreement for C_{38} , we present in Fig. 4(a) the correlation between the curvature energy $\Delta E_C^{Keating}$ and ΔE_{tot}^{DFT} based on DFT for all fullerenes discussed in Fig. 3(a). The narrow spread of the data points around the $\Delta E_C^{Keating} = \Delta E_{tot}^{DFT}$ line confirms that the continuum elasticity approach is competitive in accuracy with computationally much more involved *ab initio* calculations.

To demonstrate the generality of our approach, we extend it from near-spherical fullerenes to nanotubes with cylindrical symmetry and schwarzites with local negative Gaussian curvature. Since nanotubes and schwarzites are infinitely large, we compare stabilities on a per-atom basis in these structures. Besides results for the fullerenes

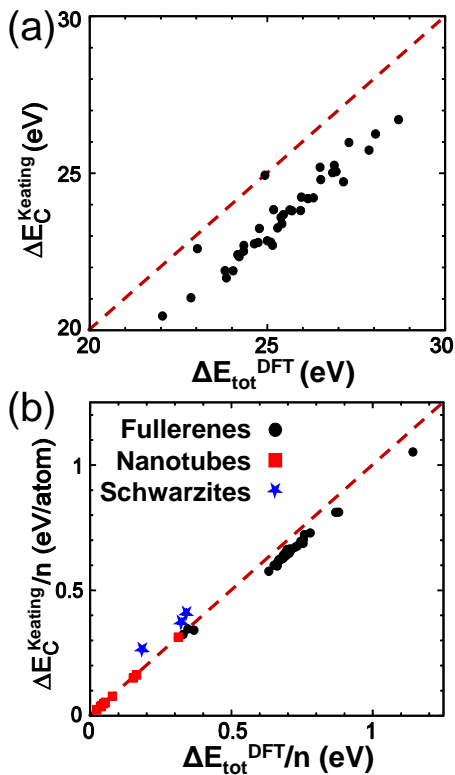


FIG. 4. (Color online) Strain energy ΔE in carbon nanostructures with respect to the graphene reference system. (a) Comparison between DFT-based total energies ΔE_{tot}^{DFT} and the curvature energy $\Delta E_C^{Keating}$ based on Keating-optimized geometries for all fullerene isomers considered in Fig. 3(a). (b) Comparison between DFT-based strain energies $\Delta E_{tot}^{DFT}/n$ and curvature energies per atom $\Delta E_C^{Keating}/n$ for Keating-optimized geometries of fullerenes, nanotubes and schwarzites. Dashed lines represent agreement between DFT and continuum elasticity results.

discussed in Figs. 3 and 4(a), Fig. 4(b) displays results for nanotubes with radii ranging between 2.5 – 9.0 Å and for schwarzite structures with 152, 192 and 200 carbon atoms per unit cell. These results again indicate an excellent agreement between curvature energies in Keating-optimized structures and DFT-based strain energies. This agreement is particularly impressive, since the spread of atomic binding energies extends over more than 1 eV.

D. Phosphorene nanotubes

As suggested at the outset, our approach to estimate relative stabilities is particularly valuable for unexplored systems such as monolayers of blue phosphorus,³⁵ where model potentials have not yet been proposed. Our DFT-PBE results for a blue phosphorene monolayer indicate $A = 4.78 \text{ \AA}^2$ as the projected area per atom, $D = 0.84 \text{ eV}$ and $\alpha = 0.10$. The monolayer structure, shown in the top

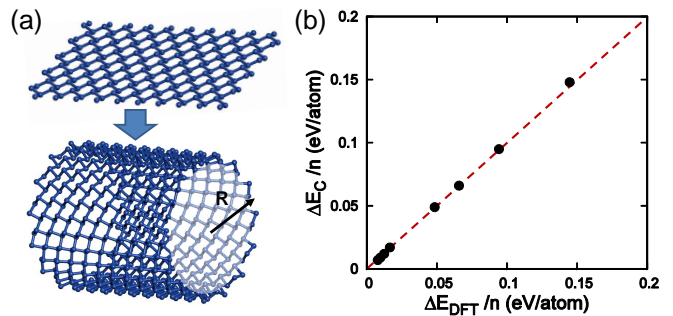


FIG. 5. (Color online) (a) Perspective view of the planar structure of a blue phosphorene monolayer (top), which has been rolled up to a nanotube with radius R (bottom). (b) Comparison between the strain energy per atom $\Delta E_C/n$ based on continuum elasticity theory and $\Delta E_{tot}^{DFT}/n$ based on DFT in blue phosphorene nanotubes. The dashed line represents agreement between DFT and continuum elasticity results.

panel of Fig. 5(a), has an effective thickness of 1.27 Å. This structure can be rolled up to phosphorene nanotubes with different radii R using the approach used in the construction of carbon nanotubes.⁷ As seen in Fig. 5(b), the strain energy for this geometry, obtained using continuum elasticity theory, agrees very well down to very small radii with results obtained using much more involved DFT calculations.³⁶

IV. DISCUSSION

Given a set of points in space, such as atomic positions, it is possible to construct a smooth surface that contains all these points in order to characterize its shape everywhere, and to eventually determine the deformation energy using the continuum elasticity approach.

We illustrate this point by tessellating the smooth surface of a graphitic nanocapsule, consisting of a cylinder capped by hemispheres at both ends and representing C_{120} , in different ways. Our results in Fig. 6 show that the average curvature energy $\langle \Delta E_C \rangle$ is rather insensitive to the tessellation density. The horizontal dashed line at $\langle \Delta E_C \rangle = 0.099 \text{ eV/\AA}^2$, representing an extrapolation to a dense tessellation, is $\approx 5\%$ higher than the exact continuum elasticity value of 0.093 eV/\AA^2 , obtained for an ideal capsule with cylinder and hemisphere radius $R = 3.55 \text{ \AA}$. The small difference arises from our approximate way to estimate the mean curvature k on the cylinder surface and at the interface between the cylinder and the hemisphere. The extrapolated value is also close to the $\langle \Delta E_{tot}^{DFT} \rangle = 0.100 \text{ eV/\AA}^2$ based on the DFT-optimized C_{120} capsule.

The reverse process to determine atomic positions from the shape alone is not unique. An informative example is the structure of a carbon nanotube. Whereas the precise atomic structure within each nanotube is defined by the chiral index, many nanotubes with different chiral indices

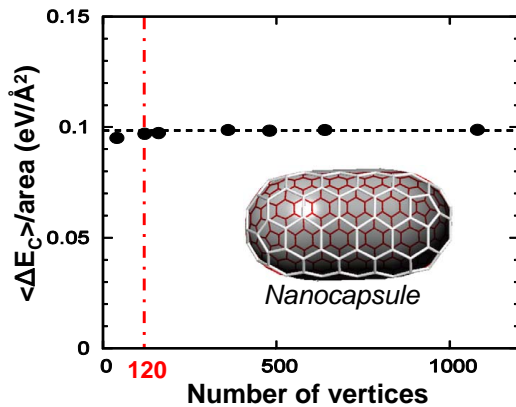


FIG. 6. (Color online) Average curvature energy $\langle \Delta E_C \rangle$ per area of a nanocapsule tessellated by a honeycomb lattice with different numbers of vertices. The vertical dash-dotted red line indicates that the capsule represents the C_{120} structure. The inset shows, how the capsule surface can be tessellated by a honeycomb lattice with 120 vertices or atoms, shown by the white lines, and also with 480 vertices, shown by the red lines. The horizontal dashed black line represents an extrapolation to an infinitely dense tessellation.

share essentially the same diameter and the same local curvature. Thus, given only the diameter of a (wide) hollow cylinder representing a nanotube, it is impossible to uniquely identify the chiral index and thus the atomic position. As a matter of fact, identifying the precise atomic positions is not necessary, since according to continuum elasticity theory, supported by experimental evidence, the stability of nanotubes depends only on the tube diameter.⁷

From its construction, the continuum elasticity description of local and global stability is best suited for very large structures with small local curvatures. Therefore, the high level of agreement between its predictions and *ab initio* results in structures with large local curvatures is rather impressive. Among the different allotropes, we find the continuum elasticity description to be most accurate for carbon nanotubes, where all bond lengths are at their equilibrium value. In fullerenes and schwarzites, the presence of non-hexagonal rings, including pentagons and heptagons, prevents a global optimization of bond lengths and bond angles, reducing the agree-

ment with DFT results.

Our stability results are consistent with the pentagon adjacency rule that provides an energy penalty of 0.7 – 0.9 eV for each pair of adjacent pentagons,^{37–39} which causes an increase of the local curvature. While this rule is surely useful, it can not compare the stability of isomers with isolated pentagons or structures of different size.

What we consider the most significant benefit of our approach to determine local strain³² is to identify the least stable sites in a structure. Local curvature and in-plane strain play the key role in both local stability and local electronic structure,⁹ which also controls the chemical reactivity.^{8,10} Thus, our approach can identify the most reactive and the least stable sites, which control the stability of the entire system.

V. SUMMARY AND CONCLUSIONS

In conclusion, we have introduced a fast method to determine the local curvature in 2D systems with arbitrary shape. The curvature information, combined with elastic constants obtained for a planar system, provides an accurate estimate of the local stability in the framework of continuum elasticity theory. Relative stabilities of graphitic structures including fullerenes, nanotubes and schwarzites, as well as phosphorene nanotubes calculated using this approach, agree closely with *ab initio* density functional calculations. The continuum elasticity approach can be applied to all 2D structures and is particularly attractive in complex systems with known structure, where the quality of parameterized force fields has not been established.

ACKNOWLEDGMENTS

We acknowledge valuable discussions with Zacharias Fthenakis. This work was funded by the National Science Foundation Cooperative Agreement #EEC-0832785, titled “NSEC: Center for High-rate Nanomanufacturing”. Computational resources for this project were provided by the Michigan State University High-Performance Computer Center.

* tomanek@pa.msu.edu

¹ K. S. Novoselov, D. Jiang, F. Schedin, T. J. Booth, V. V. Khotkevich, S. V. Morozov, and A. K. Geim, Proc. Natl. Acad. Sci. U. S. A. **102**, 10451 (2005).

² Y. Feldman, E. Wasserman, D. J. Srolovitz, and R. Tenne, Science **267**, 222 (1995).

³ H. W. Kroto, J. R. Heath, S. C. O’Brien, R. F. Curl, and R. E. Smalley, Nature **318**, 162 (1985).

⁴ S. Iijima, Nature **354**, 56 (1991).

⁵ C. Chuang, Y.-C. Fan, and B.-Y. Jin, J. Chem. Inform. Modeling **49**, 361 (2009).

⁶ A. L. Mackay and H. Terrones, Nature **352**, 762 (1991).

⁷ D. Tománek, *Guide Through the Nanocarbon Jungle* (Morgan & Claypool, 2014).

⁸ X. Lu and Z. Chen, Chem. Rev. **105**, 3643 (2005).

⁹ V. M. Pereira and A. H. Castro Neto, Phys. Rev. Lett. **103**, 046801 (2009).

- ¹⁰ J. Yang, Y. Liu, D. Zhang, X. Wang, R. Li, and Y. Li, unpublished.
- ¹¹ S. Berber and D. Tománek, Phys. Rev. B **80**, 075427 (2009).
- ¹² L. Jiao, L. Zhang, X. Wang, G. Diankov, and H. Dai, Nature **458**, 877 (2009).
- ¹³ D. V. Kosynkin, A. L. Higginbotham, A. Sinitskii, J. R. Lomeda, A. Dimiev, B. K. Price, and J. M. Tour, Nature **458**, 872 (2009).
- ¹⁴ J. Tersoff, Phys. Rev. Lett. **61**, 2879 (1988).
- ¹⁵ E. Albertazzi, C. Domene, P. W. Fowler, T. Heine, G. Seifert, C. Van Alsenoy, and F. Zerbetto, Phys. Chem. Chem. Phys. **1**, 2913 (1999).
- ¹⁶ T. G. Schmalz, W. A. Seitz, D. J. Klein, and G. E. Hite, J. Am. Chem. Soc. **110**, 1113 (1988).
- ¹⁷ H. W. Kroto, Nature **329**, 529 (1987).
- ¹⁸ D. Tomanek, W. Zhong, and E. Krastev, Phys. Rev. B **48**, 15461 (1993).
- ¹⁹ A. Enyashin, S. Gemming, and G. Seifert, Europ. Phys. J. Spec. Topics **149**, 103 (2007).
- ²⁰ A. Maceri, *Theory of Elasticity* (Springer, Berlin, 2010).
- ²¹ D. Meek and D. Walton, Computer Aided Geometric Design **17**, 521 (2000).
- ²² C. Chuang, Y.-C. Fan, and B.-Y. Jin, J. Chem. Inform. Modeling **49**, 1679 (2009).
- ²³ M. Hazewinkel, ed., *Encyclopaedia of Mathematics* (Springer, Berlin, 1995).
- ²⁴ E. Artacho, E. Anglada, O. Dieguez, J. D. Gale, A. Garcia, J. Junquera, R. M. Martin, P. Ordejon, J. M. Pruneda, D. Sanchez-Portal, and J. M. Soler, J. Phys. Cond. Mat. **20**, 064208 (2008).
- ²⁵ D. M. Ceperley and B. J. Alder, Phys. Rev. Lett. **45**, 566 (1980).
- ²⁶ J. P. Perdew and A. Zunger, Phys. Rev. B **23**, 5048 (1981).
- ²⁷ J. P. Perdew, K. Burke, and M. Ernzerhof, Phys. Rev. Lett. **77**, 3865 (1996).
- ²⁸ N. Troullier and J. L. Martins, Phys. Rev. B **43**, 1993 (1991).
- ²⁹ H. J. Monkhorst and J. D. Pack, Phys. Rev. B **13**, 5188 (1976).
- ³⁰ M. R. Hestenes and E. Stiefel, J. Res. Natl. Bur. Stand. **49**, 409 (1952).
- ³¹ P. W. Fowler and D. E. Manolopoulos, *An atlas of fullerenes*, International series of monographs on chemistry (Clarendon Press, 1995).
- ³² See Supplemental Material at <http://link.aps.org/supplemental/10.1103/PhysRevLett.000.000000> for a discussion of optimized fullerene geometries.
- ³³ P. N. Keating, Phys. Rev. **145**, 637 (1966).
- ³⁴ G. Overney, W. Zhong, and D. Tomanek, Z. Phys D: Atoms, Molecules and Clusters **27**, 93 (1993).
- ³⁵ Z. Zhu and D. Tománek, Phys. Rev. Lett. **112**, 176802 (2014).
- ³⁶ J. Guan, Z. Zhu, and D. Tománek, unpublished.
- ³⁷ B. L. Zhang, C. Z. Wang, K. M. Ho, C. H. Xu, and C. T. Chan, J. Chem. Phys. **97**, 5007 (1992).
- ³⁸ A. Warshel and M. Karplus, J. Am. Chem. Soc. **94**, 5612 (1972).
- ³⁹ F. Negri, G. Orlandi, and F. Zerbetto, Chem. Phys. Lett. **144**, 31 (1988).